Preprints of the 21st IFAC World Congress (Virtual)
Berlin, Germany, July 12-17, 2020

Virtual torque sensor for electrical bicycles

Berno J.E. Misgeld [*,**] **Lukas Bergmann** [**] **Bence Szilasi** [*]
Steffen Leonhardt [**] **Dietmar Greven** [*]

[*] *Amprio GmbH, Neuss, Germany (e-mail: berno.misgeld@de.rheinmetall.com)*
[**] *Philips Chair for Medical Information Technology, RWTH Aachen University, Aachen, Germany (e-mail: misgeld@hia.rwth-aachen.de)*

Abstract: We present a novel approach to the reconstruction of the physical pedalling torque in an electrically powered bicycle. The external force due to the road slope that is acting on the bicycle is estimated employing the reconstruction of the inclination angle with an orthogonal filter. This orthogonal filter uses an adaptive weighting between gyroscope and accelerometer sensor data. The applied weighting function is based on the bicycle's acceleration, estimated from a bicycle velocity sensor. By employing a nonlinear physical model of the bicycle, the cyclist's pedalling torque is reconstructed with an Unscented Kalman Filter. Experimental results from the inclination angle estimator and virtual torque sensor for different road slopes underline the performance of the proposed approach.

Keywords: E-bike, orthogonal filter, MEMS, Unscented Kalman Filter, bicycle, virtual sensor

1. INTRODUCTION

The density of road traffic has continuously increased in Europe in recent times. There was, for example, an increase in road traffic of kilometres travelled of 34 % from 1991 to 2016 in Germany alone (Umweltbundesamt (2019)). As a consequence, air pollution of urban areas is under ongoing public discussion. Moreover, local governments in Europe disincentivising the use of conventionally fuelled vehicles and a ban of certain vehicle classes for urban areas is discussed. Additional problems arise in urban or metropolitan areas due to increasing road traffic that is caused by parcel, express and courier services. Here, an increase in deliveries of about 7 % was observed in Germany for the year 2017.

Electrical mobility concepts were recently introduced to provide a solution to the challenges posed by public and individual transportation. Ground-based electric mobility, however, is not limited to buses, cars and trains but also single-track vehicles, such as electric bicycles play a role in modern urban traffic. Electric bicycles present a cost-effective, practical and relatively cheap alternative for short to medium travelling distances. Besides the advantage of a reduction of the environmental impact in urban areas, an electric bicycle might require the active contribution of the driver. Therefore, a health or fitness component is associated with electrical bikes, which makes them also attractive for the ageing population.

Market available electrical bicycles can be divided into two main categories. Here we refer to (a) an E-bike as an electrical bicycle that does not require the active pedalling contribution of the driver. The mechanical power may thus be fully provided by the electrical motor. The required electrical support power can be adjusted by the user of the E-bike. (b) A PEDELEC (derives from the term PEDal-ELECtric) is a bicycle that includes an electric motor that is controlled such that a mechanical support power is provided as a fraction of the driver mechanical power. In Pedelecs, the fraction of support power is called *assist ratio* and can be adjusted by the driver. Pedelecs have several advantages. Similar to purely physiologically powered bicycles, they have a small footprint, are relatively light, easy to use and there is no need for a licence or insurance. They require only a reduced physical effort, yet they are partially human-powered; so a fitness aspect can still be associated. During the last decade there was a tremendous increase in the number of sold pedelec systems in Europe and North America and the marked for pedelec systems is still growing (Simsekoglu and Klöckner (2019)).

The commercial success of Pedelecs has also lead to increased attention in the scientific community. In recent years, different Pedelec concepts were introduced and corresponding control strategies were investigated. Advanced control strategies that automatically determine the support ratio, with e.g. the objective of a longer range, were presented in Fayazi et al. (2013). Some of these studies employ physiological models of the fatigue state of the driver (Corno et al. (2016)). However, of central importance for the development of pedelec support systems, is the optimisation of the drive unit and corresponding control strategies.

Modern drive units of Pedelecs are typically equipped with a torque sensor which is able to measure the pedalling torque given by the driver. A reconstructed driver pedalling torque, based on, e.g. a model, has, therefore, the potential to save money, weight and available drive unit space. Driver pedalling torque estimation was already addressed in the literature. A study on the reconstruction of the driver torque is presented by Huang et al. (2016). The authors propose a model that is based on Newtons second law and a Luenberger observer. A disturbance

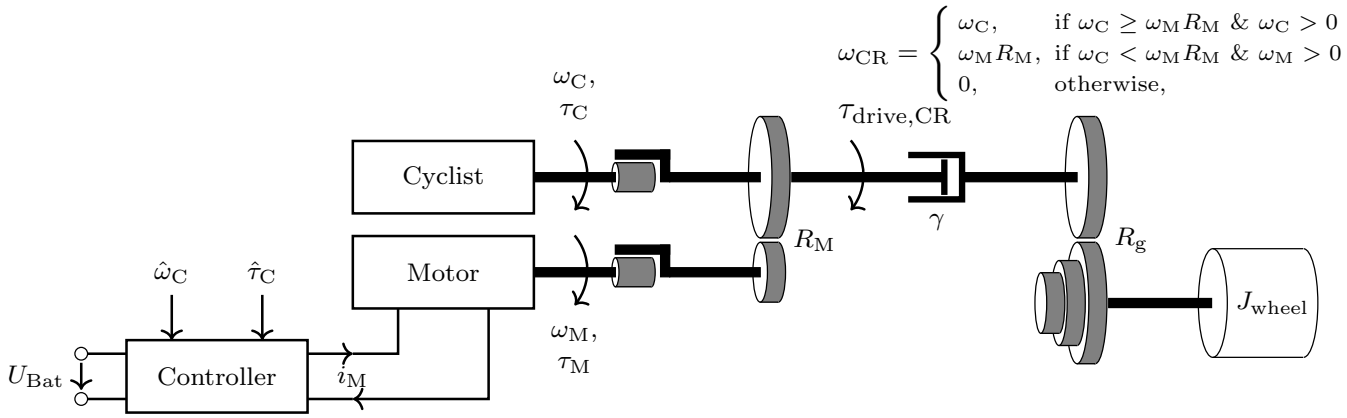

Fig. 1. Concept of Pedelec with parallel power-train (C: Cyclist, M: Motor, CR: Chain Ring, g: Hub Gear). Two freewheels decouple the rotation caused by the motor and the cyclist when the rotational speed of both differs.

observer for the reconstruction of pedalling torque is proposed in Sankaranarayanan and Ravichandran (2015). The approach is based on modelling the pedalling torque as a disturbance, to use it as a reference signal for a torque controller.

In contrast to the previous approaches, we address the reconstruction of driver pedalling torque by employing a nonlinear bicycle dynamics model. Our novel approach relies on the accurate reconstruction of the bicycle inclination angle (i.e. pitch angle) based on a drive unit micro-electro-mechanical-sensor (MEMS). An adaptive orthogonal filter is proposed (Mahony et al. (2008)), which employs the bicycle acceleration in addition to the 3-axis accelerometer and gyroscope data. An Unscented Kalman Filter (UKF) is developed that estimates the driver's pedalling torque based on a process model of an external disturbance in form of a Brownian motion.

This paper is organised as follows. In Section 2, the nonlinear bicycle model which is the basis for the UKF is introduced. Section 3 follows with the presentation of the orthogonal filter and the design of the UKF. In Section 4, simulation and experimental data are shown and discussed. Finally, Section 5 ends with a conclusion.

2. SYSTEM MODELLING

2.1 Electric drive system

A principal conceptual overview of the Pedelec drive system with a motor placed at the bottom bracket is given in Figure 1. The electrical motor is connected to the bottom bracket shaft by a gear reduction stage. Two freewheel mechanisms decouple the motor from the pedalling and the chain spider motion. The torques of the cyclist τ_C and the electrical motor τ_M are summed up to result in the torque that is transmitted to the chain via the spider $\tau_{drive,CR}$. Transmission ratios of the electrical motor and the gear hub are given by R_M and R_g, respectively. Fig. 1 also includes the controller that is used to provide supportive torque, based on measured pedalling cadence $\hat{\omega}_C$ and torque $\hat{\tau}_C$. Electrical energy is typically taken from a rechargeable battery, indicated by terminal voltage U_{Bat}. A damping of gear reduction and bearings is indicated by lumped parameter γ. Note that the rotational speed of the chain ω_{CR} depends on the pedalling motion of the driver, the motor motion and the freewheel mechanism, as indicated by the equation provided in Fig. 1.

2.2 Model equations

The main forces driving the bicycle are the torque provided by the cyclist τ_C and the torque provided by the motor τ_M. The former one results from a force the cyclist applies to the pedals, whereby the pedals are attached to the bicycle's bottom bracket via a lever arm of the length r_{pedal}. The cyclist's torque is superimposed by a torque generated by the drive unit, that is also directly applied to the chain ring:

$$\tau_{\mathrm{drive,CR}} = \tau_{\mathrm{C}} + \tau_{\mathrm{M}} \,. \tag{1}$$

The forward force that drives the bicycle is given by

$$F_{\mathrm{drive}} = \tau_{\mathrm{drive,CR}} \cdot (1-\gamma) \cdot \frac{R_g}{r_{\mathrm{wheel}}} \,, \tag{2}$$

where r_{wheel} denotes the radius of the wheel and γ accounts for losses of the torque transmitted via the chain. There are additional forces that act on the bicycle. The rolling friction force is given by (Ehsani et al. (2005))

$$F_{\mathrm{roll}}(t) = m_{\mathrm{total}} \cdot g \cdot c_r \cdot \cos(\alpha_s(t)) \,, \tag{3}$$

where $m_{\mathrm{total}} = m_{\mathrm{cyclist}} + m_{\mathrm{bike}}$ denotes the total mass of the bicycle, c_{r} is a rolling friction factor, g is the gravitational constant and α_{s} is road's slope angle. Rolling and bearing friction forces of the bicycle are modelled as (Páscoa et al. (2012))

$$\begin{aligned} F_{\mathrm{bearing}}(t) &= F_{\mathrm{b0}} + F_{\mathrm{b1}}(t) \\ &= \beta_0 + \beta_1 \cdot v_{\mathrm{bike}}(t) \end{aligned} \tag{4}$$

where the constant part is covered by β_0 and the bicycle velocity v_{bike} is multiplied by β_1. An external force is acting on the bicycle due to gravity. This force varies depending on road slope angle α_s as

$$F_{\mathrm{slope}}(t) = m_{\mathrm{total}} \cdot g \cdot \sin(\alpha_s(t)) \,. \tag{5}$$

Finally, the force due to air drag is given as

$$F_{\mathrm{air}}(t) = \frac{1}{2} \cdot c_d \cdot \rho \cdot A_{\mathrm{total}} \cdot v_{\mathrm{bike}}^2(t) \,, \tag{6}$$

and depends on drag coefficient c_d, air density ρ, total exposed frontal plane area A_{total} and the bicycle velocity above ground v_{bike}. External forces due to wind are neglected since there is no sensor available. The sum of all

forces of eqs. (2)-(6), together with the mass of inertia and the inertia of the two wheels J_{wheel}

$$m_{\text{tot}} = m_{\text{total}} + \frac{J_{wheel}}{r_{\text{wheel}}^2}\,, \tag{7}$$

leads to the nonlinear state space model

$$\begin{aligned}\dot{\boldsymbol{x}} =& \boldsymbol{f}(\boldsymbol{x},\boldsymbol{u}) = \begin{bmatrix}\dot{s}_{\text{bike}}\\ \dot{v}_{\text{bike}}\end{bmatrix}\\ =& \boldsymbol{f}\left(\begin{bmatrix}s_{\text{bike}}\\ v_{\text{bike}}\end{bmatrix}, \begin{bmatrix}\tau_{\text{C}}\\ \tau_{\text{M}}\\ \alpha_s\\ R_g\\ \beta_0\end{bmatrix}\right)\\ =& \begin{bmatrix} v_{\text{bike}} \\ \frac{1}{m_{\text{tot}}}\left(-\beta_0 - \beta_1\cdot v_{\text{bike}} - \frac{1}{2}\cdot c_d\cdot\rho\cdot A_{\text{total}}\cdot v_{\text{bike}}^2\right)\end{bmatrix}\\ &+ \begin{bmatrix} 0 \\ \frac{1}{m_{\text{tot}}}\left(-m_{\text{total}}\cdot g\cdot(c_r\cdot\cos(\alpha_s)+\sin(\alpha_s))\right)\end{bmatrix}\\ &+ \begin{bmatrix} 0 \\ \frac{1}{m_{\text{tot}}}\left(\frac{(1-\gamma)R_g}{r_{\text{wheel}}}(\tau_{\text{M}}+\tau_{\text{C}})\right)\end{bmatrix}.\end{aligned} \tag{8}$$

A subset of parameters of the dynamical bicycle model were fitted according to experimental data, recorded while pedalling on level road. In order to find the parameters, the quadratic error with respect to bicycle velocity is minimised

$$\min_{\gamma,c_r,\beta_0,\beta_1,c_d,A_{\text{total}}} \left(v_{\text{bike,meas}}(t) - v_{\text{bike,sim}}(t)\right)^2, \tag{9}$$

where $v_{\text{bike,meas}}$ is the measured velocity of the bicycle on a flat ground and $v_{\text{bike,sim}}$ is the simulated output of the model. Bicycle model parameters are given in Table A.1 in Appendix A. Figure 2 shows the results of the parameter fitted model.

3. FILTER DESIGN

3.1 Orthogonal Filter

The orthogonal filter that is employed here processes available 3-degrees of freedom (DoF) accelerometer and gyroscope measurements. The proposed filter is based on (Mahony et al. (2008)) and (Madgwick (2010)). Of special interest for the virtual torque sensor application is the pitch angle Θ which gives information about the current road slope angle. We define a positive pitch angle Θ in the opposite direction of the road slope angle α_s. A typical assumption for the reconstruction of inclination angle data from 6-DoF gyroscope/accelerometer data is that

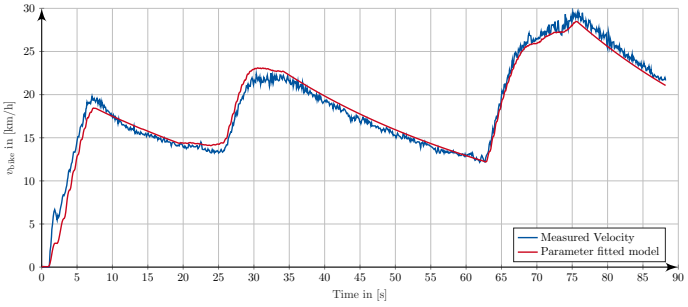

Fig. 2. Result of parameter fitting for the bicycle model (red - simulated velocity, blue - measured velocity).

the inertial measurement unit (IMU) only measures the Earth's gravity field (Madgwick (2010)). However, in the bicycle application scenario linear accelerations typically appear in acceleration or brake phases. The application of a fusion of 3-DoF accelerometer data would thus lead to an erroneous reconstruction of inclination angles in theses phases. We therefore present a new adaptive version of the orthogonal filter which weights the different orientation estimations based on the gyroscope and acceleration measurement with a sliding gain under the presence of linear accelerations. Here, we employ a high-resolution velocity sensor located in the hind wheel of the bicycle. Thus, in a first step, the acceleration of the bicycle $\hat{a}$ is estimated by using a DT1 structure

$$G_{\text{DT1}}(s) = \frac{\hat{a}(s)}{v_{\text{bike}}(s)} = \frac{1.25\cdot s}{1+1.25\cdot s}\,, \tag{10}$$

whereby the cut-off frequency of the high pass filter G_{DT1} was chosen to 1.247 rad/s. In a second step, the estimated acceleration of the bicycle $\hat{a}$ is used to calculate a weighting factor γ_a for ${}^{b}_{w}\dot{\hat{\boldsymbol{q}}}_{err,k}$:

$$\gamma_a = \begin{cases} 1, & \text{for } |\hat{a}| < 0.1\,\frac{\text{m}}{\text{s}^2}\\ -10\cdot|\hat{a}|+2, & \text{for } 0.1\,\frac{\text{m}}{\text{s}^2} < |\hat{a}| < 0.2\,\frac{\text{m}}{\text{s}^2}\\ 0, & \text{for } |\hat{a}| > 0.2\,\frac{\text{m}}{\text{s}^2}\,,\end{cases} \tag{11}$$

where ${}^{b}_{w}\dot{\hat{\boldsymbol{q}}}_{err,k}$ denotes the quaternion of the estimated error in the angular rate derived by the acceleration measurement. A block diagram showing the adaptive quaternion-based, orthogonal orientation filter is given in Figure 3. Note that the optimisation problem to compute the desired orientation ${}^{b}_{w}\dot{\hat{\boldsymbol{q}}}_{g}$ with the predefined reference direction of the gravity field in the world coordinates ${}^{w}\boldsymbol{g}$ when a normalized acceleration measurement in the body-fixed coordinates ${}^{b}\hat{\boldsymbol{a}}$ is given by

$$\min_{{}^{b}_{w}\hat{\boldsymbol{q}}_g\in\mathbb{R}^4} \boldsymbol{f}\left({}^{b}_{w}\hat{\boldsymbol{q}}_g\,,\,{}^{w}\boldsymbol{g}\,,\,{}^{b}\hat{\boldsymbol{a}}\right) \tag{12}$$

$$\boldsymbol{f}_g\left({}^{b}_{w}\hat{\boldsymbol{q}}_g\,,\,{}^{w}\boldsymbol{g}\,,\,{}^{b}\hat{\boldsymbol{a}}\right) = {}^{b}_{w}\hat{\boldsymbol{q}}_g\otimes{}^{w}\boldsymbol{g}\otimes{}^{b}_{w}\hat{\boldsymbol{q}}_g - {}^{b}\hat{\boldsymbol{a}} \tag{13}$$

$${}^{b}_{w}\hat{\boldsymbol{q}}_g = [q_0\ q_1\ q_2\ q_3]^T \tag{14}$$

$${}^{w}\boldsymbol{g} = [0\ 0\ 0\ 1]^T \tag{15}$$

$${}^{b}\hat{\boldsymbol{a}} = [0\ a_x\ a_y\ a_z]^T\,. \tag{16}$$

3.2 Torque estimation

For an estimation of the torque, the model dynamics of eq. (8) was extended with an additional acceleration state a_C that is caused by the pedal torque, as generated by the driver. This additional input is acting on the acceleration summation point and is driven by a white noise process $\dot{a}_C = w_3$. Given an estimation of the acceleration caused by the cyclist makes it possible to calculate a torque $\hat{\tau}_{\text{C}}$ that is required to cause such an acceleration:

$$\hat{\tau}_{\text{C}} = \frac{r_{\text{wheel}}J_{\text{total}}}{(1-\gamma)\cdot R_g}a_{\text{C}}\,. \tag{17}$$

The nonlinear Euler discretised dynamical system is given

$$\begin{aligned}\boldsymbol{x}_k =& \boldsymbol{f}(\boldsymbol{x}_{k-1},\boldsymbol{u}_k) + \boldsymbol{w}_k\\ \begin{bmatrix}x_{s,k}\\ x_{v,k}\\ x_{a_C,k}\end{bmatrix} =& \boldsymbol{f}\left(\begin{bmatrix}x_{s,k-1}\\ x_{v,k-1}\\ x_{a_C,k-1}\end{bmatrix}, \begin{bmatrix}\tau_{\text{M}}\\ \alpha_s\\ R_g\\ \beta_0\end{bmatrix}\right) + \boldsymbol{w}_k\,,\end{aligned} \tag{18}$$

where the nonlinear output function can be described by:

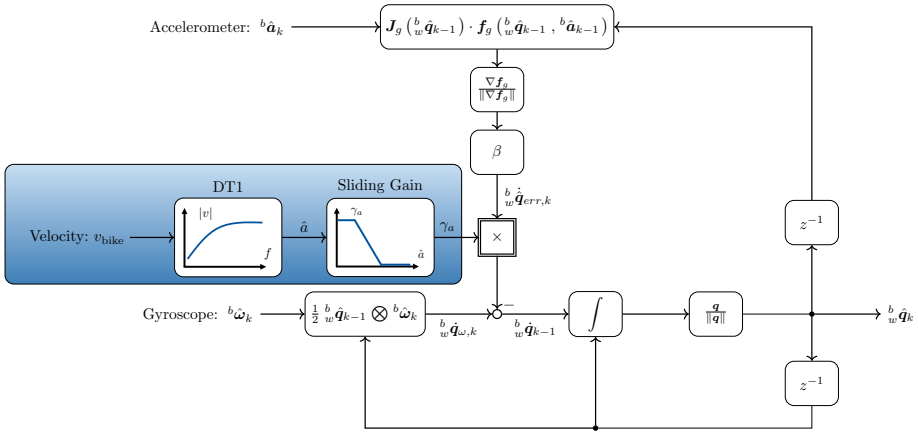

Fig. 3. Quaternion-based, orthogonal orientation filter with Gauss-Newton optimization.

$$\begin{aligned}\boldsymbol{z}_k =&\boldsymbol{h}(\boldsymbol{x}_k,\boldsymbol{u}_k)+\boldsymbol{v}_k\\ \begin{bmatrix}z_{s,k}\\ z_{v,k}\\ z_{a,k}\end{bmatrix} =& \begin{bmatrix}s_{\text{bike},k}\\ v_{\text{bike},k}\\ a_{\text{bike},k}\end{bmatrix} = \boldsymbol{h}\left(\begin{bmatrix}x_{s,k}\\ x_{v,k}\\ x_{a_C,k}\end{bmatrix},\begin{bmatrix}\tau_{\text{M}}\\ \alpha_s\\ R_g\\ \beta_0\end{bmatrix}\right)+\boldsymbol{v}_k\,.\end{aligned}\tag{19}$$

The parameters $\boldsymbol{w}$ and $\boldsymbol{v}$ represent zero-mean, uncorrelated white Gaussian noise processes with

$$E\left\{\begin{bmatrix}\boldsymbol{w}_i\\ \boldsymbol{v}_i\end{bmatrix}\begin{bmatrix}\boldsymbol{w}_j^T & \boldsymbol{w}_j^T\end{bmatrix}\right\}=\begin{bmatrix}\boldsymbol{Q} & \boldsymbol{0}\\ \boldsymbol{0} & \boldsymbol{R}\end{bmatrix}\delta_{ij}\,.\tag{20}$$

In eq. (20), $\boldsymbol{Q}$ and $\boldsymbol{R}$ are the corresponding covariance matrices, and δ_{ij} denotes the Kronecker delta function. For the UKF in this work, the following process noise and measurement noise covariance matrices are proposed

$$\boldsymbol{Q}=\boldsymbol{\Sigma}_{x,0}=\begin{bmatrix}0.01 & 0 & 0\\ 0 & 0.01 & 0\\ 0 & 0 & 0.01\end{bmatrix},\ \boldsymbol{R}=\begin{bmatrix}0.001 & 0 & 0\\ 0 & 0.001 & 0\\ 0 & 0 & 0.1\end{bmatrix},\tag{21}$$

whereby the initial state guess covariance $\boldsymbol{\Sigma}_{x,0}$ is chosen equal to the process noise covariance. The choice of $\boldsymbol{Q}$ and $\boldsymbol{R}$ is motivated as follows. A measurement for the acceleration of the bicycle in driving direction can either be given by the accelerometer of the IMU and subtracting the gravity vector or by calculating the abbreviation of the measured velocity of the bicycle. Either way, the measurement of the acceleration has a higher error than the measurement of the velocity or the distance. Therefore, the measurement noise covariance for the acceleration measurement $R_{3,3}$ is chosen two powers of ten bigger than the one for the velocity $R_{1,1}$ and the distance measurement $R_{2,2}$. Furthermore, the noise in the acceleration measurement should be filtered out, which is why $Q_{3,3}$ was chosen ten times smaller than $R_{3,3}$. Nevertheless, the state estimation should respond quickly, especially for changes in the velocity. Therefore, $Q_{1,1}$ and $Q_{2,2}$ were chosen ten times bigger then $R_{1,1}$ and $R_{2,2}$. With these covariance matrices, a fast response of the estimated velocity is expected, while the estimation of the cyclist's acceleration is expected to have a low-pass filtered behaviour.

The UKF was implemented in Matlab/Simulink according to (Julier and Uhlmann (2004)). In a first step, the sigma points $\mathscr{X}_{i,k-1}$ and the weightings $W_i^{m,c}$ $(i\in(1\ldots2N))$ are calculated. The free parameters in the scaling factor $\lambda=\alpha^2(N+\kappa)-N$ and β were chosen as suggested in (Wan and Van Der Merwe (2000)): $\alpha=10^{-4}$ (a small positive value), $\kappa=0$ and $\beta=2$. The UKF's sample time was chosen as $\Delta t=50$ ms motivated by the update time of the velocity v_{bike} and the commanded motor current i_{M}.

4. EXPERIMENTAL RESULTS

The Pedelec used in this study is a 28-inch touring bicycle with a hub gear. Figure 4 shows a picture of the test bicycle. The test bicycle is equipped with a battery, an operating panel and a Pedal-electric drive unit (Amprio GmbH, Neuss, Germany). Communication between drive unit and operating panel/battery is realised via the CAN-bus. The bicycle is also equipped with a BeagleBone Blue board (BeagleBone Blue, BeagleBoard.org, Michigan, USA), a 3-DoF accelerometer and 3-DoF gyroscope (5MPU-9250 InvenSense Inc., San Jose, USA) and a GPS sensor (GLOBALSAT GPS Module EM-506, Globalsat Technology Corporation, Hsien, Taiwan). The BeagleBone Blue is connected via the CAN-bus and serves as a computation platform and data logging device. In a first test, the bicycle is driven on flat ground which leads to a short ramp, after which flat ground follows. The length (hypotenuse) of the ramp is given with 9.5 m and the height is 1.33 m. This complies with a road slope angle of 8.05° (or 14 % inclination). The road section in front of the ramp was leading gently uphill ($\alpha_s=0.7°$), while the road section behind the ramp was leading with the same angle downhill ($\alpha_s=-0.7°$). For the validation run, the ramp was cycled upwards at an average velocity

Fig. 4. Picture of the test bicycle.

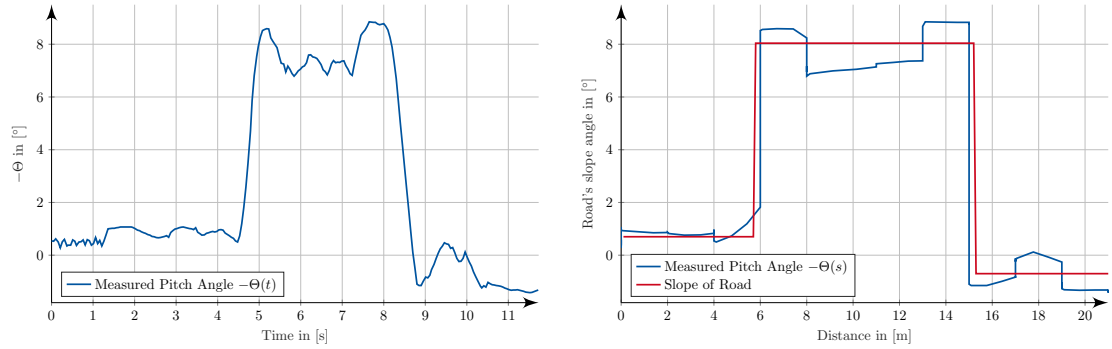

Fig. 5. On the left: Pitch angle measurement depending on the time while cycling uphill on a ramp with a road slope angle of 8.05°. On the right: The same measurement is shown in blue but depending on the distance, additionally, the estimated reference is given by the red curve.

of 8.6 km/h. During this run, the bicycle's pitch angle was estimated over the time on the BeagleBone using the adaptive orientation filter. The measurement data of this experiment is shown in Figure 5. Note the reversed sign between the pitch angle Θ and the road slope angle α_s. For the right subplot in Figure 5, the pitch angle was transformed such that it is a function of the distance instead of the time in order to make the reference and the estimated orientation comparable. The root mean square error between the reference slope angle and the negative pitch angle $-\Theta$ was calculated to $\mathrm{RMS}(\Theta, \alpha_s) = 1.2°$. Furthermore, the resolution of the bicycle's odometer is only provided in integer values of 1 m, which is also the reason for the small discontinuities in the blue graph of the right subplot.

Additional acceleration and deceleration experiments were conducted with the adaptive filter. The maximum errors and RMS errors during the three different phases - acceleration, constant velocity and deceleration - are provided in Table B.1, Appendix B assuming a road slope angle of $\alpha_s = 0$. The maximum error during the constant velocity is caused by a street bump. The RMS error during acceleration and deceleration can be lowered with the modified orientation filter by more than 2°, while the RMS error during a constant velocity slightly increases by 0.2°.

An example result of an acceleration-deceleration test is shown in Figure 6. As described in Section 3.1, the velocity measurement is used to estimate the acceleration with a DT1 high pass structure. This estimation $\hat{a}$ is visualized in the second subplot of the same figure. Whenever the estimated acceleration $\hat{a}$ is outside the dashed red lines, the modified orientation estimation only takes the gyroscope measurement into account in order to prevent an error-prone estimation due to linear acceleration. The calculated pitch angle Θ of the bicycle is presented in the third subplot of Fig. 6. Whereby, the pitch angle was calculated twice, first, by using the modified orientation filter that takes the estimated acceleration $\hat{a}$ into account (blue line in third subplot). Secondly, by using the unmodified orientation filter according to (Madgwick (2010)) (red line in third subplot). The real road slope angle in this test was assumed to be $\alpha_s = 0$. It can be observed that the pitch angle estimated with the unmodified filter reaches a value of $\Theta = 3.49°$ during acceleration, whereby the modified orientation estimates a pitch angle close to zero.

Similar results can be observed during deceleration. In the last subplot of Fig. 6 the measured (blue) and estimated (red) cyclist's torque is shown. The input to the UKF is the estimated acceleration $\hat{a}$, the measured velocity v_{bike} and the measured traveled distance s_{bike}. An additional input to the UKF is the estimated pitch angle, whereby the pitch angle from the orientation filter is not directly used, but instead a moving average $\bar{\Theta}$ with a window size of 5 s in order to filter out any bumps and vibrations due to uneven ground. During the acceleration phase, it can be observed that the estimated torque using the UKF directly responds to the increasing velocity. Additionally, it can be seen that the estimated torque follows an approximated average mean value of the measured torque. Therefore, for validation purposes, it is proposed not to calculate the RMS error between the real measured torque but instead to calculate the RMS between the estimated torque and a moving average $\bar{\tau}_{\mathrm{C}}$ of the measured torque with a sliding window size of 0.7 s. This RMS error for the time from the start of the acceleration until the start of the deceleration phase is calculated to: $\mathrm{RMS}(\hat{\tau}_{\mathrm{C}}, \bar{\tau}_{\mathrm{C}}) = 10.1$ Nm. During the deceleration phase, it can be seen that the UKF also estimates negative torque corresponding to the break force the cyclist applies through the breaks.

5. CONCLUSION

The proposed UKF for the nonlinear bicycle model is able to reconstruct the driver pedalling torque by introducing a novel adaptive orthogonal filter, that is tailored to this application. However, a trade-off needs to be made. On the one hand, the estimation of the pitch angle should be robust under the presence of high vibrations and road bumps. On the other hand, high dynamics are required in the pitch angle estimation in order to provide a good torque estimation with the UKF as there are fast changes in the road's slope angle. Nevertheless, the developed UKF is a promising approach that could replace the torque sensor in the bicycle to save costs.

REFERENCES

Corno, M., Berretta, D., Spagnol, P., Savaresi, S. M., 2016. Design, control, and validation of a charge-sustaining parallel hybrid bicycle. IEEE Transactions on Control Systems Technology 24 (3), 817–829.

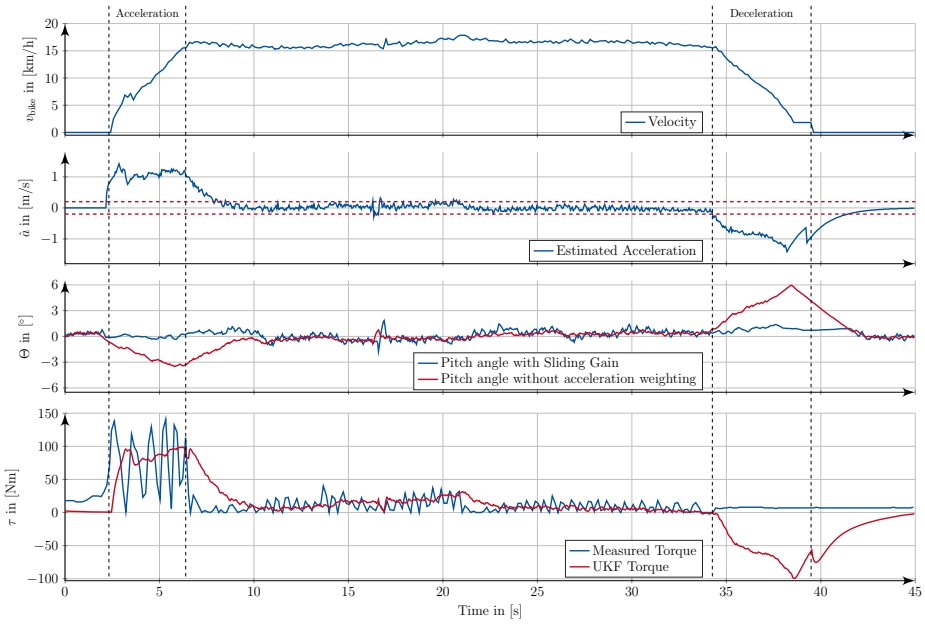

Fig. 6. Orientation and estimated torque while cycling on flat ground. First subplot: measured acceleration; second subplot: estimated acceleration; third subplot: pitch angles; fourth subplot: pedaling torque.

Ehsani, M., Gao, Y., Gay, S., Emadi, A., 2005. Modern electric, hybrid electric and fuel cell vehicles fundamentals, theory and design, crc press.

Fayazi, S. A., Wan, N., Lucich, S., Vahidi, A., Mocko, G., 2013. Optimal pacing in a cycling time-trial considering cyclist's fatigue dynamics. In: American Control Conference (ACC), 2013. IEEE, pp. 6442–6447.

Huang, C.-F., Dai, B.-H., Yeh, T.-J., 2016. Observer-based sensor fusion for power-assist electric bicycles. American Control Conference (ACC), 5486–5491.

Julier, S. J., Uhlmann, J. K., 2004. Unscented filtering and nonlinear estimation. Proceedings of the IEEE 92 (3), 401–422.

Madgwick, S., 2010. An efficient orientation filter for inertial and inertial/magnetic sensor arrays. Report x-io and University of Bristol (UK) 25, 113–118.

Mahony, R., Hamel, T., Pflimlin, J., June 2008. Nonlinear complementary filters on the special orthogonal group. IEEE Transactions on Automatic Control 53 (5), 1203–1218.

Páscoa, J., Brójo, F., Santos, F., Fael, P., 2012. An innovative experimental on-road testing method and its demonstration on a prototype vehicle. Journal of Mechanical Science and Technology 26 (6), 1663 – 1670.

Sankaranarayanan, V., Ravichandran, S., 2015. Torque sensorless control of a human-electric hybrid bicycle. International Conference on Industrial Instrumentation and Control (ICIC), 806–810.

Simsekoglu, Ö., Klöckner, C., 2019. Factors related to the intention to buy an e-bike: A survey study from norway. Transportation Research Part F: Traffic Psychology and Behaviour 60, 573–581.

Umweltbundesamt, 2019. Fahrleistungen, Verkehrsaufwand und Modal Split.

Wan, E. A., Van Der Merwe, R., 2000. The unscented kalman filter for nonlinear estimation. In: Adaptive Systems for Signal Processing, Communications, and Control Symposium. pp. 153–158.

Appendix A. BICYCLE MODEL PARAMETERS

Table A.1. Identified parameters for the bicycle model.

Name	Parameter	Value	Unit
Mass of bicycle and cyclist	m_{total}	95	kg
Earth's gravity	g	9.81	$\frac{\text{m}}{\text{s}^2}$
Air density	ρ	1.2	$\frac{\text{kg}}{\text{m}^3}$
Wheel radius	r_{wheel}	0.3683	m
Chain wheel & gear loss	γ	0.09	-
Rolling friction coefficient	c_r	0.006	-
Bearing resistance coefficient	β_0	0.15	N
Bearing resistance coefficient	β_1	1.497	$\frac{\text{N s}}{\text{m}}$
Aerodynamic drag coefficient	c_d	0.4	-
Exposed frontal plane	A_{total}	0.5	m^2
Pedal momentum arm length	r_{pedal}	0.175	m

Appendix B. MAXIMUM RMS ERRORS

Table B.1. Maximum and RMS errors for the unmodified and modified orientation estimation.

	$\max\lvert\Theta - \alpha_s\rvert$		$\text{RMS}(\Theta, \alpha_s)$	
	unmodified	modified	unmodified	modified
Accel.	3.49°	0.77°	2.38°	0.22°
Const. vel.	0.86°	1.84°	0.34°	0.54°
Accel.	5.95°	1.38°	3.82°	0.84°